



This is a repository copy of *Earlier collapse of Anthropocene ecosystems driven by multiple faster and noisier drivers*.

White Rose Research Online URL for this paper:

<https://eprints.whiterose.ac.uk/200848/>

Version: Published Version

---

**Article:**

Willcock, S. [orcid.org/0000-0001-9534-9114](https://orcid.org/0000-0001-9534-9114), Cooper, G.S. [orcid.org/0000-0001-6268-6608](https://orcid.org/0000-0001-6268-6608), Addy, J. et al. (1 more author) (2023) Earlier collapse of Anthropocene ecosystems driven by multiple faster and noisier drivers. *Nature Sustainability*. ISSN 2398-9629

<https://doi.org/10.1038/s41893-023-01157-x>

---

**Reuse**

This article is distributed under the terms of the Creative Commons Attribution (CC BY) licence. This licence allows you to distribute, remix, tweak, and build upon the work, even commercially, as long as you credit the authors for the original work. More information and the full terms of the licence here:

<https://creativecommons.org/licenses/>

**Takedown**

If you consider content in White Rose Research Online to be in breach of UK law, please notify us by emailing [eprints@whiterose.ac.uk](mailto:eprints@whiterose.ac.uk) including the URL of the record and the reason for the withdrawal request.



[eprints@whiterose.ac.uk](mailto:eprints@whiterose.ac.uk)  
<https://eprints.whiterose.ac.uk/>

# Earlier collapse of Anthropocene ecosystems driven by multiple faster and noisier drivers

Received: 19 October 2022

Simon Willcock<sup>1,2,7</sup>✉, Gregory S. Cooper<sup>3,4,7</sup>, John Addy<sup>5</sup> & John A. Dearing<sup>6</sup>

Accepted: 24 May 2023

Published online: 22 June 2023

 Check for updates

A major concern for the world's ecosystems is the possibility of collapse, where landscapes and the societies they support change abruptly. Accelerating stress levels, increasing frequencies of extreme events and strengthening intersystem connections suggest that conventional modelling approaches based on incremental changes in a single stress may provide poor estimates of the impact of climate and human activities on ecosystems. We conduct experiments on four models that simulate abrupt changes in the Chilika lagoon fishery, the Easter Island community, forest dieback and lake water quality—representing ecosystems with a range of anthropogenic interactions. Collapses occur sooner under increasing levels of primary stress but additional stresses and/or the inclusion of noise in all four models bring the collapses substantially closer to today by ~38–81%. We discuss the implications for further research and the need for humanity to be vigilant for signs that ecosystems are degrading even more rapidly than previously thought.

For many observers, UK Chief Scientist John Beddington's argument that the world faced a 'perfect storm' of global events by 2030<sup>1</sup> has now become a prescient warning. Recent mention of 'ghastly futures'<sup>2</sup>, 'widespread ecosystem collapse'<sup>3</sup> and 'domino effects on sustainability goals'<sup>4</sup> tap into a growing consensus within some scientific communities that the Earth is rapidly destabilizing through 'cascades of collapse'<sup>5</sup>. Some<sup>6</sup> even speculate on 'end-of-world' scenarios involving transgressing planetary boundaries (climate, freshwater and ocean acidification), accelerating reinforcing (positive) feedback mechanisms and multiplicative stresses. Prudent risk management clearly requires consideration of the factors that may lead to these bad-to-worst-case scenarios<sup>7</sup>. Put simply, the choices we make about ecosystems and landscape management can accelerate change unexpectedly.

The potential for rapid destabilization of Earth's ecosystems is, in part, supported by observational evidence for increasing rates of change in key drivers and interactions between systems at the global scale (Supplementary Introduction). For example, despite decreases in global birth rates and increases in renewable energy generation, the general trends of population, greenhouse gas concentrations and

economic drivers (such as gross domestic product) are upwards<sup>8,9</sup>—often with acceleration through the twentieth and twenty-first centuries. Similar non-stationary trends for ecosystem degradation<sup>10</sup> imply that unstable subsystems are common. Furthermore, there is strong evidence globally for the increased frequency and magnitude of erratic events, such as heatwaves and precipitation extremes<sup>11</sup>. Examples include the sequence of European summer droughts since 2015<sup>12</sup>, fire-promoting phases of the tropical Pacific and Indian ocean variability<sup>13</sup> and regional flooding<sup>11</sup>, already implicated in reduced crop yields<sup>14</sup> and increased fatalities and normalized financial costs<sup>9</sup>.

The increased frequency and magnitude of erratic events is expected to continue throughout the twenty-first century. The Intergovernmental Panel on Climate Change (IPCC) Sixth Assessment Report concludes that 'multiple climate hazards will occur simultaneously, and multiple climatic and non-climatic risks will interact, resulting in compounding overall risk and risks cascading across sectors and regions'<sup>11</sup>. Overall, global warming will increase the frequency of unprecedented extreme events<sup>11</sup>, raise the probability of compound events<sup>15</sup> and ultimately could combine to make multiple system failures

<sup>1</sup>Net Zero and Resilient Farming, Rothamsted Research, Harpenden, UK. <sup>2</sup>School of Natural Sciences, Bangor University, Bangor, UK. <sup>3</sup>Institute for Sustainable Food, University of Sheffield, Western Bank, Sheffield, UK. <sup>4</sup>Department of Geography, University of Sheffield, Western Bank, Sheffield, UK.

<sup>5</sup>Intelligent Data Ecosystems, Rothamsted Research, Harpenden, UK. <sup>6</sup>Geography and Environmental Science, University of Southampton, Southampton, UK. <sup>7</sup>These authors contributed equally: Simon Willcock, Gregory S. Cooper. ✉e-mail: [simon.willcock@rothamsted.ac.uk](mailto:simon.willcock@rothamsted.ac.uk)

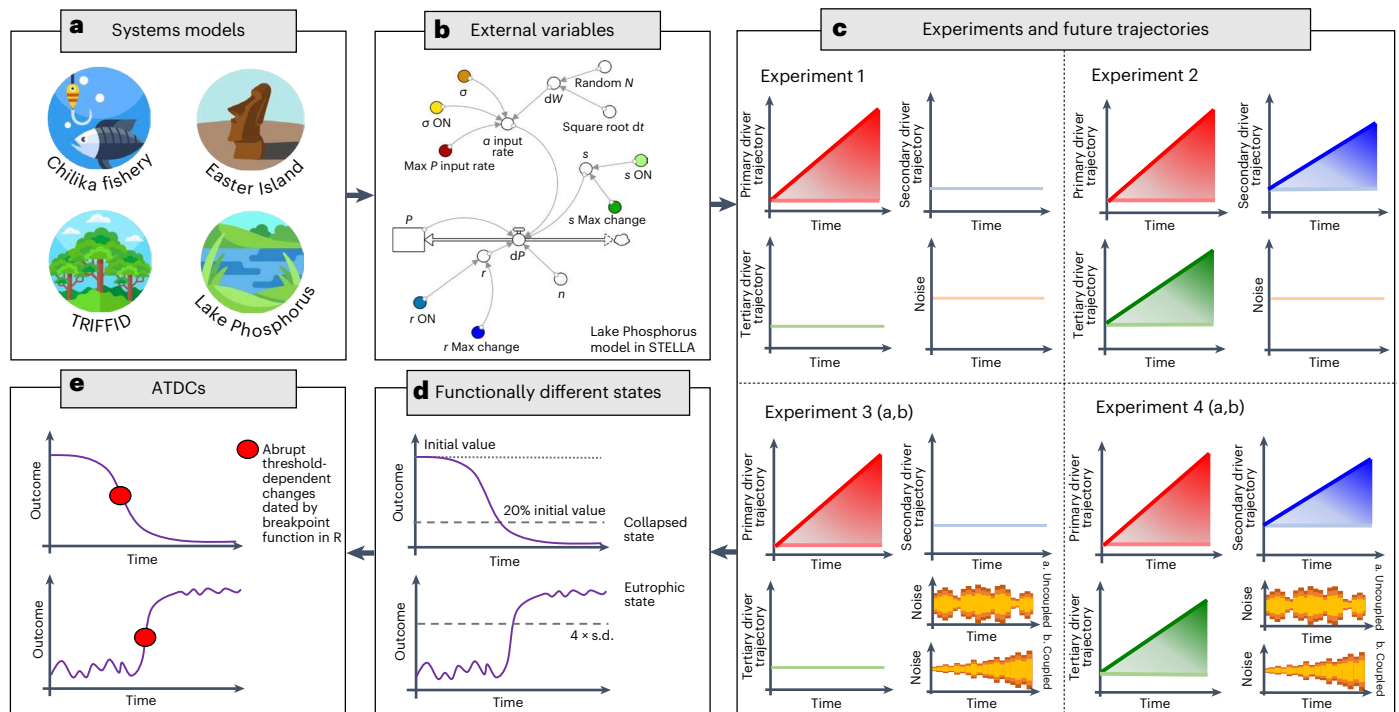


**Fig. 1 | Schematic overview of the framework developed to explore the influence of slow driver trajectories and/or noise on the timing of ATDCs.**

**a**, The four systems models simulated in this study (see section on Overview of systems models). **b**, Schematic representation of a system dynamics model (Lake Phosphorus model) with its external slow (blue and green) and noisy (red/orange) drivers depicted in colour (see Generation of future scenarios). **c**, Depiction of the four experiment types (section on Generation of future scenarios), ranging from changes in the primary baseline driver only (experiment 1), changes in all slow drivers and noise inputs simultaneously (experiment 4, where ‘a’ and ‘b’ represent noise profiles that are uncoupled or coupled to the primary driver

trajectory, respectively): darker colours schematically represent steeper trajectories and/or higher noise levels. **d**, The two linear techniques used to check whether outcomes shift into a functionally different state (section on Time-series breakpoint detection)—the top panel is applied to Lake Chilika, Easter Island and TRIFFID, where the systems collapse from high quantitative outcome states to low quantitative outcome states and the bottom panel is applied to Lake Phosphorus (where lake phosphorus concentrations shift from low to high). **e**, Depiction of the time-series breakpoint date recognition (section on Time-series breakpoint detection). The Easter Island icon in **a** is made by Roundicons and the remaining three icons are made by Freepik, as sourced from [www.flaticon.com](http://www.flaticon.com).

more likely<sup>16</sup>. For example, there is a risk that many tipping points can be triggered within the Paris Agreement range of 1.5 to 2 °C warming, including collapse of the Greenland and West Antarctic ice sheets, die-off of low-latitude coral reefs and widespread abrupt permafrost thaw<sup>17</sup>. These tipping points are contentious and with low likelihood in absolute terms but with potentially large impacts should they occur. In evaluating models of real-world systems, we therefore need to be careful that we capture complex feedback networks and the effects of multiple drivers of change that may act either antagonistically or synergistically<sup>18–20</sup>. Prompted by these ideas and findings, we use computer simulation models based on four real-world ecosystems to explore how the impacts of multiple growing stresses from human activities, global warming and more interactions between systems could shorten the time left before some of the world’s ecosystems may collapse.

Intuitively, stronger interactions between systems may be expected to increase the numbers of drivers of any one system, change driver behaviour and generate more system noise. As a result, we would anticipate that higher levels of stress, more drivers and noise may bring forward threshold-dependent changes more quickly. For any particular system (for example, the Amazon forest) it is possible to envisage a time sequence that starts with one main driver (for example, deforestation), then multiple drivers (for example, deforestation plus global warming), more noise through extreme events (for example, more droughts and wildfires), with additional feedback mechanisms that enhance the drivers (for example, diminished internal water cycle and more severe droughts). A vortex could therefore emerge, with drivers generating noisier systems as climate variability and the incidence of extreme events increases. Under worst-case scenarios, the circle becomes faster

as reinforcing feedbacks accelerate connections or human activities increase stress levels. However, extreme events could also counteract each other (for example, extreme droughts and extreme rainfall events) and interconnections could also have weakening effects (for example, where increased plant growth driven by increased CO<sub>2</sub> is counterbalanced by increased temperatures and droughts). To date, there is limited observational evidence showing that ecosystems have a record of tipping between alternate stable states<sup>21</sup>.

Others<sup>19</sup> offer a mathematical tripartite classification of critical transitions that includes slow driver bifurcations, rate-induced (fast/cumulative driver) and noise-induced (extreme event) tipping points. However, previous studies tend to focus on each of these categories individually. For example, there is a well-established body of physics and mathematical theory on ‘mean exit times’<sup>22</sup>, with studies investigating the timing of tipping points in rate-induced<sup>18–20</sup> or noisy<sup>19,23,24</sup> systems. However, despite calls for more experimental evidence of the impacts of climate variability and extremes on ecosystems<sup>25,26</sup>, the relative importance or combined effect of fast drivers, multiple drivers and noisy system drivers on the collapse of real-world ecosystems is not known. Critical transitions driven by current pollution forcings such as greenhouse gas emissions<sup>27</sup> and nutrient loadings<sup>28</sup> are likely to be new, well beyond the envelope of natural variability. Hence, we avoid the use of the terms critical transition and tipping points, used formally in dynamical systems theory to represent shifts to alternative attractors and focus on abrupt threshold-dependent changes (ATDCs) that would be perceived by society as the quantitative (for example, fish and stock integrity) and/or qualitative (for example, ecosystem functions) collapse of a desirable system state<sup>29,30</sup>.

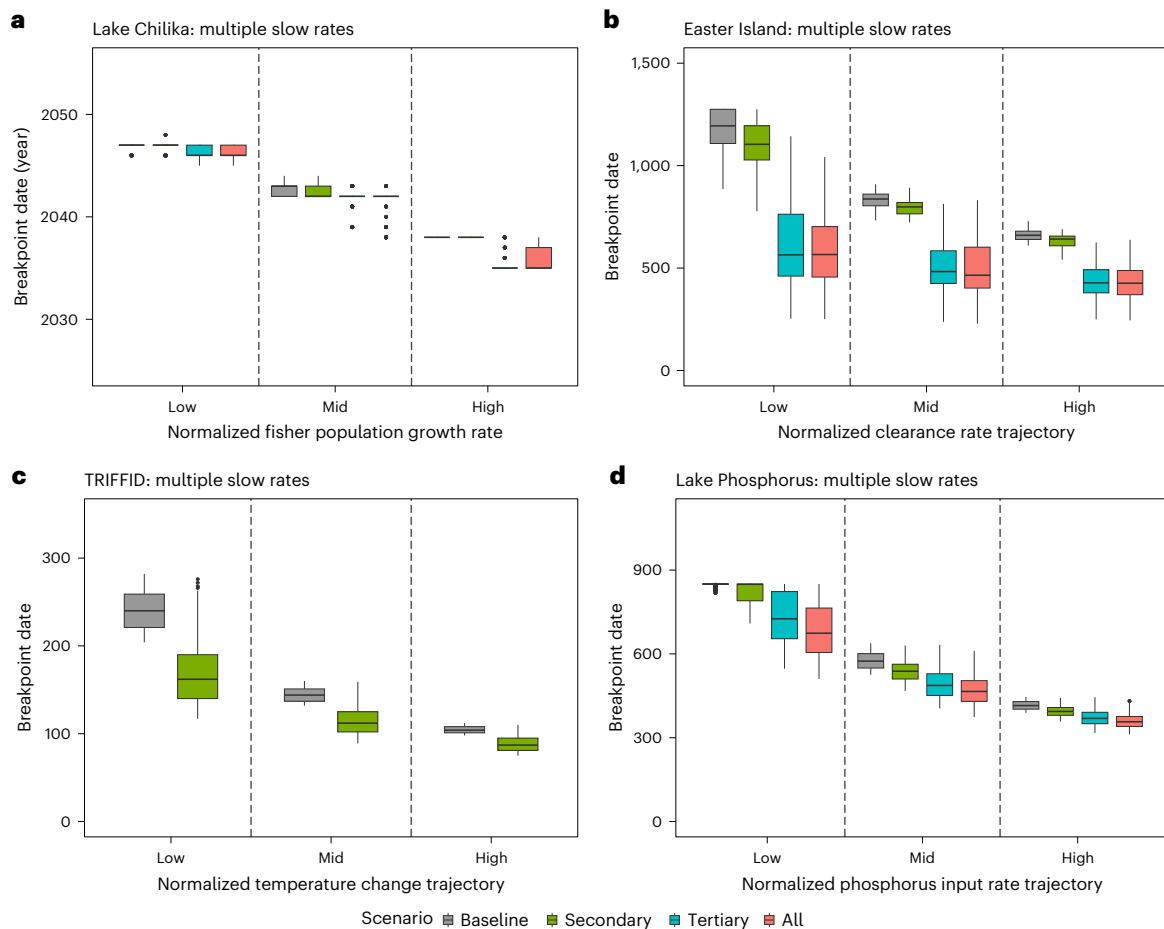


**Fig. 2 | The relationship between the breakpoint date and the primary (baseline) slow driver for the individual (grey) and multiple (coloured) drivers.** The normalized primary driver trajectories are apportioned into three discrete ranges: low, 0.25–0.35; mid, 0.45–0.55; and high, 0.65–0.75. **a–d**, Subplots: Lake Chilika model, primary slow driver—fisher population growth, secondary driver—climate change, tertiary driver—fish price (**a**); Easter Island model, primary slow driver—tree clearance, secondary driver—agricultural carrying capacity, tertiary driver—tree mortality (**b**); TRIFFID model, primary slow driver—temperature change, secondary driver—disturbance rate (**c**);

Lake Phosphorus model, primary slow driver—phosphorus external input, secondary driver—phosphorus recycling rate, tertiary driver—phosphorus sedimentation rate (**d**). Model timestep units: Lake Chilika, Easter Island and TRIFFID run in years; timesteps in Lake Phosphorus are unitless. Boxplots depict the median (50th percentile), upper quartile (75th percentile) and lower quartile (25th percentile); individual points represent outliers which fall outside  $1.5\times$  the interquartile range from the lower and upper quartiles (as depicted by the boxplot whiskers). See Supplementary Table 3-1 for the number of model simulations underpinning each boxplot.

We have selected a range of system dynamic models that have been previously used to demonstrate generalizable findings (for example, with regard to safely overshooting ATDCs<sup>27</sup>) and can be externally manipulated to simulate internal emergent ATDCs at local and regional scales—as if they were impacted through stronger connections to other systems. Reflecting modern ecosystems, these models show varied anthropogenic interactions, ranging from social-ecological systems with strongly coupled human–nature feedbacks to ecological systems with predominantly one-way interactions where ecosystems are influenced by the external impacts of people. The ability of these models to capture feedback loops, delays and interactions between components is well established<sup>31,32</sup> and has motivated their use in various recent studies of sustainability and resilience<sup>21,33–35</sup>. Therefore, guided by the ref. 19 typology of tipping points, we aim to generalize the dynamics of increasing the numbers of drivers, their rates and variability (as proxies for stronger interactions between systems and noise) on the speed at which ATDCs are reached in four ecosystem dynamics models (Fig. 1): Lake Chilika lagoon fishery<sup>21,33</sup>, Easter Island<sup>36</sup>, Lake Phosphorus<sup>28,37</sup> and a modified version of The Hadley Centre Dynamic Global Vegetation Model (TRIFFID) of forest dieback<sup>27,38</sup>.

## Results

As described in the Methods, the four models each have a primary (baseline) slow driver (Fig. 2, grey boxplots), where linear changes in their trajectories over time can initiate ATDCs in their respective outcome variable (Lake Chilika, fish population; Easter Island, human population; TRIFFID, tree coverage; Lake Phosphorus, lake phosphorus concentration). When the strength of the primary slow driver in each model is increased, the modelled systems collapse sooner—as defined by a statistical breakpoint in their temporal trends (section on Time-series breakpoint detection). Increasing the strength of multiple drivers with additional secondary and tertiary drivers further reduces the breakpoint date (Fig. 2), with variation around these median responses determined by the relative strength of the additional drivers—with addition of a weak secondary driver bringing forward the start of system collapse substantially less than the addition of a strong secondary driver (Supplementary Fig. 2-1).

In addition to earlier breakpoint dates, extra drivers can also cause ATDCs at levels where it would be resilient to the primary slow driver in isolation (Supplementary Section 2). For example, across the 1,000 timesteps of the Lake Phosphorus model, the system is stable at normalized baseline driver rates up to 0.348 (that is, Lake Phosphorus

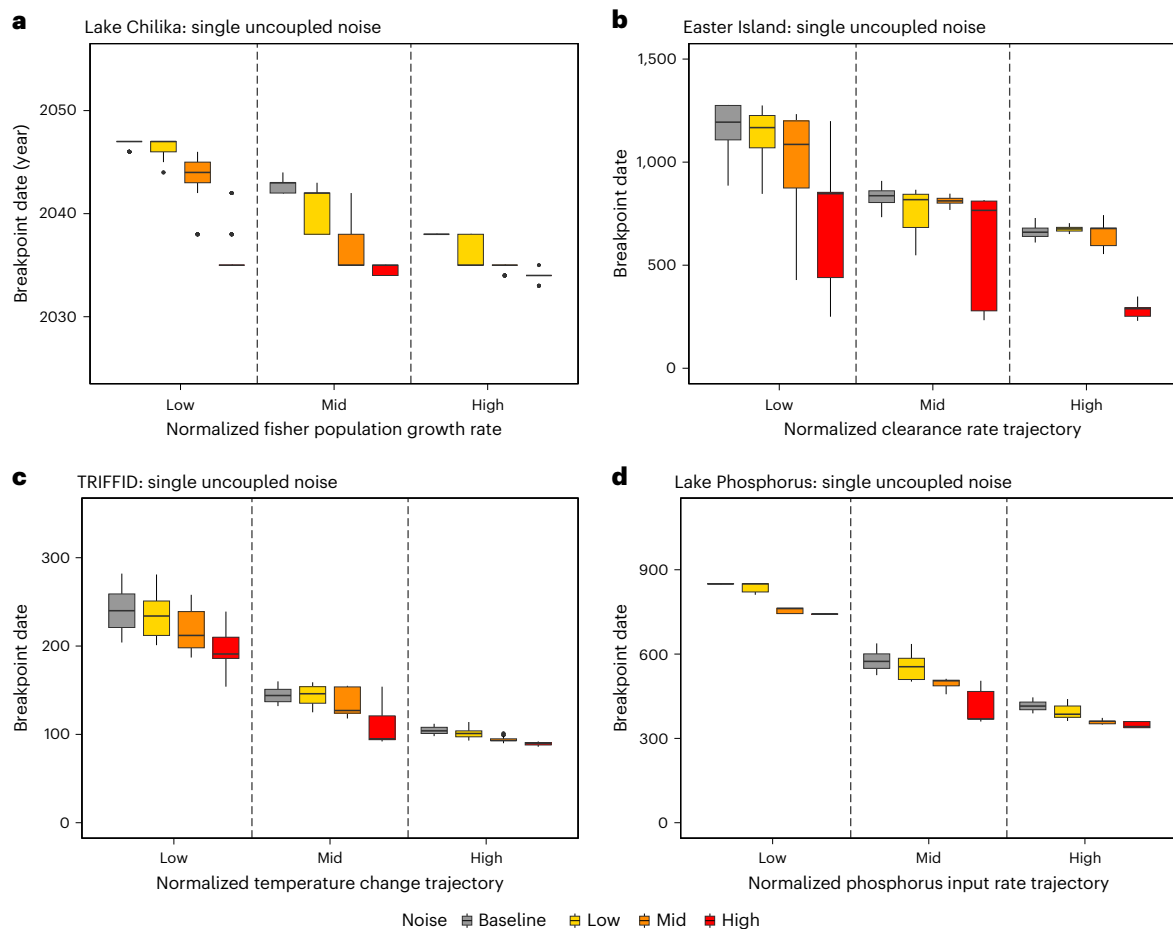


**Fig. 3 | The relationship between the breakpoint date and the primary slow driver (grey) for varying levels of uncoupled noise in the primary slow driver.** Where normalised primary slow driver ( $\sigma$ ) values  $\leq 0.333$  signify 'low noise' (yellow), normalised  $\sigma$  values  $> 0.333$  and  $\leq 0.666$  signify 'mid noise' (orange), and normalised  $\sigma$  values  $> 0.666$  signify 'high noise' (red; section on Generation of future scenarios). The normalized primary driver trajectories are apportioned into three discrete ranges: low–0.25–0.35, mid–0.45–0.55 and high–0.65–0.75.

**a–d**, Subplots: Chilika model outputs, primary slow driver–fisher population growth (a); Easter Island model outputs, primary slow driver–tree clearance (b); TRIFFID model outputs, primary slow driver–temperature change (c); Lake Phosphorus model outputs, primary slow driver–phosphorus input (d). Model timestep units and boxplot dimensions are the same as in Fig. 2; see Supplementary Table 3-1 for the number of model simulations underpinning each boxplot.

concentration does not go through a breakpoint; Supplementary Fig. 2-4d). However, the addition of a single secondary driver of normalized strength 0.3 can lead to breakpoints occurring at normalized primary driver strengths 0.312 (reduction from baseline: 0.036 (10.3%); Supplementary Fig. 2-4d) and the addition of an extra tertiary driver with normalized strength 0.3 can lead to breakpoints at normalized primary strengths 0.270 (reduction from baseline: 0.078 (22.4%); Supplementary Fig. 2-4d). With all additional drivers, 12.3% of breakpoints observed in the Lake Phosphorus model occurred at primary driver strengths below the minimum threshold required to result in a breakpoint when the primary driver is acting in isolation (Lake Chilika, 1.2%; Easter Island, 14.8%; TRIFFID, 7.7%; Supplementary Table 2-1).

Next, for each of the four models, the trajectories of the primary slow drivers were randomly perturbed by the addition of noise (section on Generation of future scenarios). Noise was generated within the system dynamics software used to run the models (STELLA<sup>39</sup>) by randomly sampling per timestep from a normal distribution with a mean value of 0 and standard deviation of  $\sigma$ , meaning that random perturbations on the system could work in both positive ( $\sigma > 0$ ) and negative directions ( $\sigma < 0$ ). The value of  $\sigma$  was randomly sampled once per simulation to explore the effects of different noise scales on the time to reach the breakpoint date (section on Generation of future scenarios). The addition of high noise (normalized  $\sigma > 0.666$ )

shows that increasing the variability of the primary slow driver (in isolation) across all four models can bring forward the date of system collapse (Fig. 3).

The effects outlined above are synergistic—combining multiple drivers with noise further reduces the breakpoint date beyond the effects of either multiple drivers or noise acting alone (Fig. 4). For example, at a normalized slow baseline driver strength of 0.3 in the Easter Island model (Fig. 4b), the addition of low uncoupled noise (normalized  $\sigma \leq 0.333$ ) with all possible additional drivers switched on with normalized strengths of over 0.666 ('high' secondary and tertiary trajectories) brings the median breakpoint forward from timestep 1,179 to timestep 426 (63.8% reduction), whereas high noise levels (defined as normalized  $\sigma > 0.666$ ) brings the breakpoint forward from timestep 1,179 to timestep 225 (80.9% reduction). The finding that the breakpoint date is most advanced by the combination of high noise and high secondary trajectories is consistent across the other three models, with the median breakpoint date at a normalized slow baseline driver strength of 0.3 changing from year 2047 to year 2035 (37.5% reduction) for Lake Chilika, timestep 238 to timestep 92 (61.3% reduction) for TRIFFID and timestep 848 to timestep 388 (54.2% reduction) for Lake Phosphorus. Across all combinations of noise and multiple drivers, 1.7%, 7.5%, 6.6% and 8.9% of modelled breakpoints occurred at primary driver strengths below the minimum threshold required to result in a breakpoint when

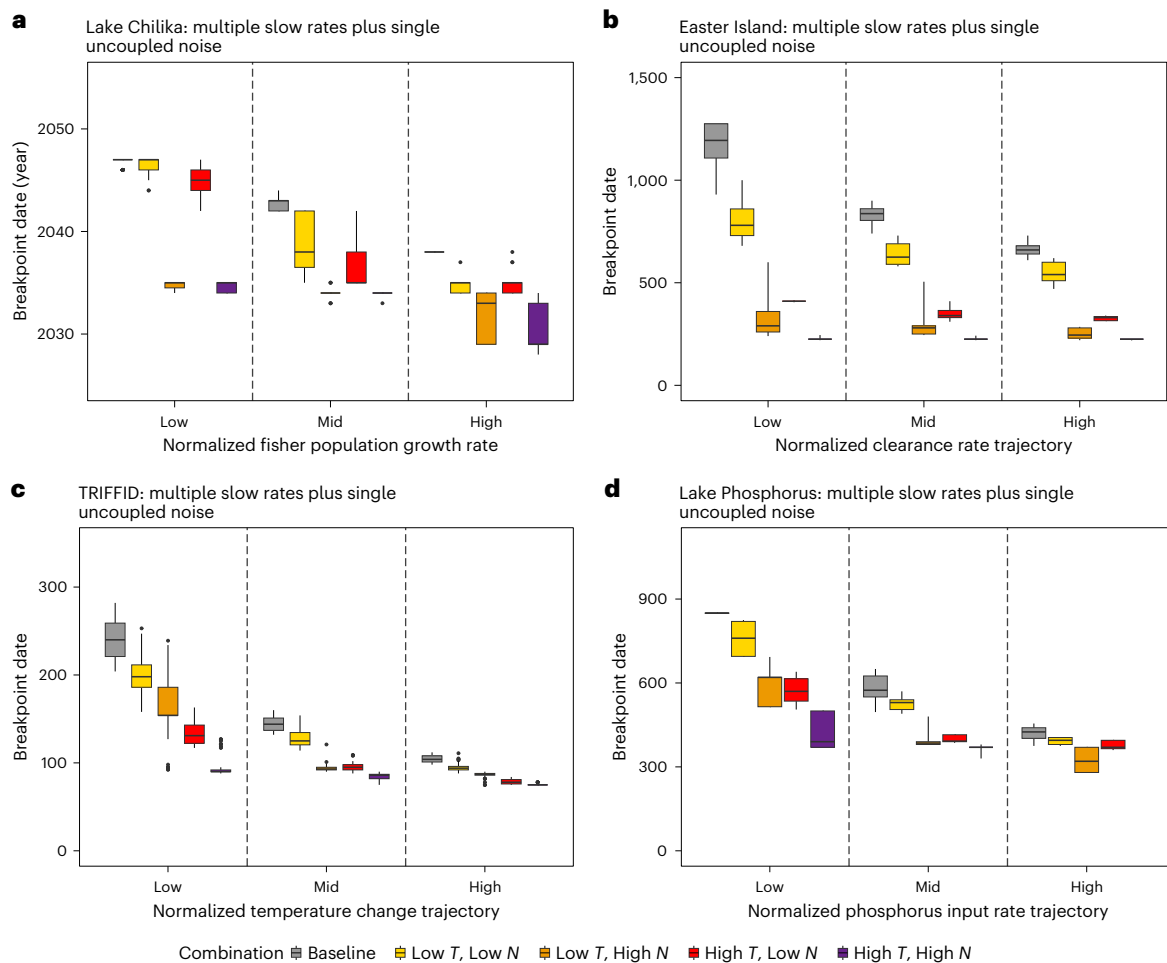


**Fig. 4 | The relationship between the breakpoint date and the primary slow driver (grey) when weak and strong multiple driver trajectories are combined with weak and strong uncoupled noise ( $N$ ).** Where normalized driver trajectories ( $T$ )  $\leq 0.333$  are classified as weak and  $T > 0.666$  as strong, similarly, normalized noise ( $\sigma$ ) values  $\leq 0.333$  and  $> 0.666$  are classified as weak and strong, respectively. The normalized primary driver trajectories are apportioned into three discrete ranges: low—0.25–0.35, mid—0.45–0.55 and high—0.65–0.75. **a–d**, Subplots: the Chilika model, primary slow driver—fisher population growth, additional driver—climate change and fish price (**a**); the Easter Island model, primary slow driver—tree clearance, additional drivers—

agricultural carrying capacity and tree mortality (**b**); the TRIFFID model, primary slow driver—temperature change, additional driver—disturbance rate (**c**); the Lake Phosphorus model, primary slow driver—phosphorus, additional drivers—phosphorus recycling rate, phosphorus sedimentation rate (**d**). Note, the Lake Phosphorus model (**d**) did not produce any outcomes between the 0.65–0.75 primary driver range within the ‘high trajectory, high noise’ scenario; however, the median breakpoint date of the adjacent range (0.55–0.65) is 346. Model timestep units and boxplot dimensions are the same as in Fig. 2; see Supplementary Table 3-1 for the number of model simulations underpinning each boxplot.

acting in isolation for Lake Chilika, Easter Island, TRIFFID and Lake Phosphorus, respectively (Supplementary Table 2-4).

All results presented above are robust to different modelling and monitoring decisions. For example, these results are consistent regardless of whether the noise is coupled to (allowed to grow with) the magnitude of the primary slow driver or uncoupled and sampled from a constant distribution (Supplementary Figs. 2-2 and 2-3 and Supplementary Tables 2-3 to 2-5) and irrespective of whether linear, nonlinear or threshold-type boundaries<sup>40</sup> are used to define the breakpoints (Supplementary Section 4 and Supplementary Figs. 4-1 to 4-6).

## Discussion

Previous findings have supported the idea that Earth’s subsystems may interact to the extent that an abrupt shift in one raises the probability that a shift may occur in another<sup>41–43</sup>. In this paper, we have explored, through four ecosystem models, how these interactions may alter the timing of ATDCs through the effects of strengthened drivers, multiple drivers and higher internal variability or noise. The potential effects are substantial with combinations of a strengthened

main driver, an additional driver and noise giving at least 38–81% reductions in the future date of a predicted ATDC compared to estimates for a non-interacting system with a constant single driver and no noise. Importantly, the effect per unit time on bringing forward an ATDC is greatest at low driver trajectories, which further strengthens the suggestion that abrupt Earth system changes may occur sooner than we think (Supplementary Introduction). Our findings also show that 1.2–14.8% of ATDCs can be triggered by additional drivers and/or noise below the threshold of driver strengths required to collapse the system if only a single driver were in effect.

Overall, we find that, as the strength of a main driver increases, the systems collapse sooner. Adding multiple drivers brings collapses further forward, as does adding noise, and the two effects can be synergistic. However, the relative importance of these changes varies across systems. For the Chilika fishery, the most influential driver is captured as the primary driver and so additional drivers have limited influence, with the addition of noise in the primary driver bringing the breakpoint date much closer to the present. For Easter Island, TRIFFID and Lake Phosphorus, the opposite is true—the addition of high levels

of noise in the primary driver advances the date of system collapse far less than additional drivers. Thus, while the earliest collapses in all the systems are found when both additional drivers and noise are applied, an important implication for real-world governance is that the precise importance of individual driver trajectories and noise is system-dependent.

### Earlier occurrence of abrupt threshold-dependent changes

Our results show that systems do not collapse at a constant level of cumulative stress (that is, total stress built up over time) irrespective of the rate of stress change (Supplementary Section 5) but rather underline the importance of rate over accumulated stress<sup>18–20</sup>. Simulations where the primary, secondary or tertiary drivers change more rapidly tend to shift earlier and are less able to absorb cumulative stress (Supplementary Fig. 5-1). Thus, the same ecosystem can collapse as a result of sustained/cumulative pressure of a slower driver but will probably collapse faster if the rate of change is increased<sup>18–20</sup>. Increasingly fast driver rates will eventually overwhelm the ability of balancing feedback loops to compensate for increased stress on the system; thus, signifying a loss of resilience. In the absence of strong balancing loops, a fast driver allows reinforcing feedback loops to grow (Supplementary Section 6). The driver may also re-energize dormant reinforcing feedback loops or allow new coupled, reinforcing feedback mechanisms to emerge (compare ref. 44). For the Easter Island, TRIFFID and Lake Phosphorus models, as the balance of feedback loops shifts towards reinforcing loops, the probability that the system will be driven out of its attractor into an ATDC increases (Supplementary Section 6). Additional drivers limit further the balancing ability of balancing feedback loops and increase the probability of collapse. For Lake Chilika, the pre-ATDC phase is dominated by reinforcing feedback loops driving fisher population growth towards dangerous levels, with collapse coinciding with the growth of balancing feedbacks in the form of reduced fish populations. These rebalance the system by limiting the effectiveness of the fisher population's fishing efforts (Supplementary Fig. 6-1).

In our analysis, the rise in driver stress is continuous over time. Where the stress is applied in discrete events (for example, wildfire events), the same response can be expected where elapsed time between events is insufficient for balancing feedback loops to rebalance the system or where large stress events motivate additional amplifying loops. This is similar to the impact of extreme events (that is, noise; Figs. 3 and 4), which has the ability to push a system out of its attractor temporarily or permanently; an effect that strengthens as the system becomes increasingly sensitive to perturbations close to a potential ATDCs<sup>19,23</sup>. However, sequences of extreme events from multiple drivers, such as extreme drought followed by extreme rainfall, may only act antagonistically where sufficient time allows for the system to repair the extreme impacts. Our study only looks at driver noise; there could coincidentally or equally be natural 'state' change/noise (vertical axis on phase-plot figures)—for example, natural tree mortality, natural lake infilling, fluctuating populations in ecosystems, or ageing population, behavioural/psychological changes in the social domain—all of which could alter the probability of ATDCs even in the absence of, or changes in, the external drivers<sup>19,23</sup>.

### Moving forward

These results have research implications for further developing and applying models of ecosystems to study ATDCs. Whilst our findings derive from models based on real-world systems, the greater complexity of reality may limit the transferability of our results. The Lake Chilika model is the most complex of the four models, with upwards of 100 model variables capturing hydroclimatic, ecohydrological, fishery and socio-economic dynamics interacting to create four balancing loops and seven reinforcing loops—and is validated against historical data<sup>33</sup>. Of all the models, it shows the least dramatic reductions in the date of any ATDC (Supplementary Introduction). Therefore, it is plausible

that more complex systems will have stronger regulating mechanisms that stabilize the system through sets of balancing feedback loops<sup>44</sup>, constraining the more extreme of our findings.

Mechanistically, in simpler models, such as the Lake Phosphorus model, regime shifts may be triggered by a single feedback loop. In more complex models (and probably ecosystems), our analysis of feedback strengths shows evidence for an instability cascade through the system via multiple feedback loops. For example, the collapse in the Easter Island human population reflects the cumulative effects of several feedback loops triggered by overharvesting the tree population, rat population and agricultural carrying capacity (Supplementary Fig. 6-2), allowing the reinforcing loop for the decline in human population to strengthen. In general, increasing driver strengths can trigger these mechanisms earlier, whereas additional drivers have the ability to shift the nature of the cascade (for example, including/excluding different feedbacks; Supplementary Figs. 6-5 to 6-8). However, in spatial terms, multiple interacting feedback mechanisms may lead to spatial re-organization which slows the rate of collapse<sup>45,46</sup>, with stochasticity promoting temporal stability—particularly in local regions with small populations<sup>24</sup>. There is the possibility, too, that interconnections could have weakening effects and, where the impacts are slower than the system response, extreme events could counteract each other. Thus, our quantitative findings could be viewed as representing worst-case scenarios for the different ecosystems<sup>7</sup>.

Nevertheless, the finding that additional stress produces qualitatively similar emergent phenomena in a range of simulation models should not be dismissed lightly<sup>47,48</sup>. The consistency across models representing varying processes, interactions and contexts may indicate that equifinality makes the accurate representation of internal system dynamics less important than the external drivers/stresses in simulating complex realities<sup>49</sup>. Clearly, model development is required to better capture the diversity of system elements, interactions and feedbacks for more complex systems and, in particular, more realistic coupling of human decision-making and ecological/environmental dynamics. With the exception of Lake Chilika<sup>33</sup>, each model in this study was originally created to study the impact of a primary driver influenced by predominantly external anthropogenic processes, presumably the driver perceived as the most impactful. Our results show that this assumption may not be the case (for example, Easter Island) and models should include a range of plausible drivers and scenario combinations if they are to avoid underestimating the risk of ATDCs. Moreover, new ecosystem models should allow for the growth of feedback loops and long-term simulations to observe the mechanisms that underpin ATDCs<sup>48,50</sup>. For example, more realistic social-ecological coupling may lead to shifts in the human decisions capable of either shifting an ATDC much closer to the present or avoiding it completely. Monitoring of real-world systems should therefore capture multiple plausible drivers, their variability and their feedbacks to social systems. More ATDCs will occur unexpectedly if the focus on perceived main drivers ignores other drivers that increase cumulative stress and gradually reduce the resilience of systems, as exemplified in the lake water regime shift at Erhai, western China<sup>28</sup>. There, abrupt lake eutrophication was initially perceived to have been driven by transgression of a threshold in nutrient enrichment driven by agricultural runoff but historical analysis has shown that the shift was also affected by lake water-level management, seasonal climate and fish farming<sup>44</sup>.

Substantial research has focused on identifying early warning metrics linked to critical slowing down theory which applies primarily to 'equilibrium' system states with single, slow drivers<sup>31</sup>. If, as we indicate, real-world tipping elements are more likely to be driven by multiple, fast drivers and extreme events, it is less likely that early warning signals in the frequency domain will be observed<sup>20,51</sup> for noise-induced thresholds. Certainly, excluding noise from model systems, whilst a potentially useful simplification for theoretical understanding, risks

creating a false sense of security by overestimating the distance remaining before critical thresholds are breached in the real world where multiple drivers and noise are abundant<sup>27,52</sup>. Therefore, alternative approaches to identifying resilience loss in real systems before ATDCs through structural metrics<sup>53–55</sup> and early warning signals generated by agent-based models<sup>50</sup> should be considered more widely.

Previous studies of interactions between tipping elements have focused on large-scale systems and suggest substantial social and economic costs from the second half of the twenty-first century onwards<sup>42,56</sup>. Our findings suggest the potential for these costs to occur sooner. For example, it is not clear whether the IPCC estimate for a tipping point in the Amazon forest before 2100 (ref. 11) includes the possibility for interacting drivers and/or noise; if not, our findings suggest that a breakdown may occur several decades earlier (Supplementary Introduction). This would occur where local-scale failures in elements (such as species populations, fish stocks, crop yields and water resources) combine with more extreme events (such as wildfires and droughts) to precondition the large-scale system, already vulnerable to the influence of other large-scale tipping elements, to collapse earlier—a meeting of top-down and bottom-up forces (Supplementary Introduction). This vertical integration of forces is reinforced by the rising trend in global warming that already represents a spatial integrator which may be expected to strengthen before it subsides. Clearly, climate economics need to incorporate these synergistic and cumulative effects that are occurring at local and regional scales into larger scale models where they are currently lacking<sup>57,58</sup>. The dominance of accelerating trends in global time series of economic consumption (for example, refs. 9,59) makes our finding that ramping up the main driver is the easiest way to bring forward an ATDC particularly worrying. Similarly, the implication for regions experiencing more extreme events is that an ATDC may occur even before the main driver has ramped up.

The commonality of findings across four well-studied ecosystems has potentially profound implications for our perception of future risks associated with the climate and ecological crises. While it is not currently possible to predict how climate-induced ATDCs and the effects of local human actions on ecosystems connect across temporal and spatial scales, our findings show the potential for each to reinforce the other. The ability of present policy and practice to prevent an ever-deepening vortex of degradation in local and regional ecosystems requires urgent investigation<sup>7</sup>.

## Methods

### Overview of systems models

Here, we briefly describe the four previously published models used to investigate the effects of multiple drivers and noise upon the timing of ATDCs. Each model was replicated and simulated within the system dynamics software STELLA Architect v.1.6.1 (ref. 39), with outputs exported into CSV files as time series and analysed in the statistical software R v.4.1.0 (ref. 60). The models, example data and code used in the analyses are available via <https://doi.org/10.5281/zenodo.7946433>.

The Lake Chilika fishery model<sup>21,33</sup> is a social-ecological model designed to simulate the future fish population and catch trajectories of the Chilika lagoon, Odisha, India. The model is able to explore the impacts of many slower drivers (fisher population growth and increased rainfall and temperatures under climate change) and many faster drivers (abrupt changes in fish prices and fishing gear) on the sustainability and resilience of the fish population until 2100. As described in detail in ref. 33, the model includes coupling between many social and ecological components of the system. First, the efficiency of fish catch efforts is proportional to the fish population density within the lagoon (as fish density declines, catch per unit effort also decreases). Second, as a form of environmental carrying capacity, the fisher population growth is proportional to the total number of livelihoods supportable by the overall fishery value, which is derived from the total fish catch in any given month. Third, fishers may invest their fishing revenues into

more intensive fishing gear (motorboats), which also has implications for fish catch and fish stock health over time. The model is also able to simulate many natural resource governance approaches (for example, fishing quotas and alternative livelihoods), although the model runs conducted here are all under the baseline governance scenario<sup>33</sup> (the tidal outlet between the lagoon and the Bay of Bengal is re-opened every 10 years to rejuvenate fish migration and lagoon salinity). The model has been previously validated against empirical data through standard behaviour-matching techniques and Monte Carlo sensitivity analysis<sup>33</sup>. The Lake Chilika model is run for a total of 1,536 timesteps (months), with each time series aggregated to the annual scale (about 1973–2100). Future trajectories, detailed in the section below on (Generation of future scenarios), activate from timestep 504 (January 2015) after the completion of the historical parameterization and validation periods<sup>33</sup>.

The Easter Island model aims to explore alternative hypotheses behind the collapse of the Easter Island civilization<sup>36</sup>. The initial parameterization of the model here is the same as the ‘ecocide’ configuration detailed in ref. 36. The main internal social-ecological feedback driving model dynamics is the balancing feedback between human population growth, tree coverage and land clearance, whereby the overharvesting of the primary resource (palm forest) can lead to overshoot dynamics and the eventual demise of the human population (ecocide). As noted in ref. 36: ‘While it is obvious that the islanders were not directly living from palm trees, the forest provided several valuable and difficult to substitute ecological services, including food from fruits and palm nuts, timber to construct houses and sea-going canoes for fishing’. In addition to this main internal social-ecological feedback, many external variables can be modified to change the speed of human population growth, including the tree clearance rate per capita, the maximum carrying capacity of the agricultural system (to help support human population growth) and the mortality rate of trees (representative of potential disease outbreaks). The model is run for 1,500 timesteps (years), with future scenarios active from the first timestep (Generation of future scenarios).

The TRIFFID model is a modified version of The Hadley Centre Dynamic Global Vegetation Model, originally developed by ref. 38 to explore the effects of atmospheric CO<sub>2</sub> concentrations on the rate of Amazon dieback. Here, we simulate the modified version developed by ref. 27, which is based around a central Lotka–Volterra equation describing the change in vegetation coverage as the primary external driver (local atmospheric temperatures) increases. On any given timestep, the change in vegetation coverage ( $dv/dt$ ) is driven by a temperature-dependent growth term and an externally set disturbance rate:

$$\frac{dv}{dt} = gv(1 - v) - yv \quad (1a)$$

$$g = g_0 \left[ 1 - \left( \frac{T_l - T_{opt}}{\beta} \right)^2 \right] \quad (1b)$$

$$T_l = T_f + (1 - v)\alpha \quad (1c)$$

Where  $v$  is the vegetation coverage (ranging from 0–100%),  $T_f$  is the temperature forcing parameter (see below),  $g$  is the vegetation growth rate (the increase in vegetation coverage [ $v$ ]),  $g_0$  is the maximum growth rate (set at 2% per year),  $y$  is the disturbance rate (see below),  $T_l$  is the local temperature,  $T_{opt}$  is the optimal temperature (28 °C),  $\beta$  is the half-width of the growth versus temperature curve (10 °C) and  $\alpha$  is the difference in temperature between surface bare soil and forest (5 °C). Therefore, the growth term is assumed to be parabolic with the local temperature (equation (1b)), meaning that once the local temperature increases beyond the optimal temperature, negative tree growth ensues (that is, additional tree mortality<sup>27</sup>), which in turn leads to an



increase in temperature (equation (1c)), which may eventually produce the runaway loss in tree coverage. Although the meaning of the disturbance rate is not specified by ref. 27, it may proxy human-induced ecosystem stresses such as deforestation for agricultural land and disease-driven forest dieback. The model is run for 500 timesteps, with future trajectories active from the first timestep (Generation of future scenarios).

The Lake Phosphorus model is a simplified version of the original ‘lake response to P input and recycling’ model<sup>37</sup>, as modified by ref. 28. The model is designed as a simple ecosystem model, with lake water phosphorus concentration driven by a generic external phosphorus input (which may, for example, proxy external inputs from agricultural runoff, sewage and industrial discharges from factories, construction sites and urban areas)<sup>61</sup>. In turn, lake water phosphorus is recycled back into the system as an ecological reinforcing feedback loop, proportional to the lake phosphorus concentration on any given timestep. Phosphorus is also removed from lake waters via sedimentation, where the volume removed in sediment is proportional to the phosphorus concentration of the lake. Therefore, on any given timestep, the change in lake phosphorus concentration ( $dP/dt$ ) equals:

$$dP = \left[ a - sP + r \frac{P^n}{P^n + 1^n} \right] dt \quad (2)$$

Where  $P$  is phosphorus concentration,  $a$  is phosphorus input rate,  $r$  is the maximum recycling rate,  $s$  is the phosphorus loss rate,  $n$  is the strength of the recycling response to phosphorus concentrations ( $n = 8$ ) and  $t$  is time (see below). The model is run for 1,000 timesteps (unitless), with future scenarios active from the first timestep (see below). Given the simplicity of this model, an area for future research could be expanding the original model to explore how adaptive management mechanisms may help to avoid ecosystem thresholds, for example, by linking government fertilizer incentives to lake phosphorus levels as the ecosystem approaches a threshold.

### Generation of future scenarios

Using the above models, we performed four *in silico* experiments (presented visually in Fig. 1):

- Experiment 1: only the primary slow driver in each model changes over time and all other drivers remain constant (Fig. 2 baseline).
- Experiment 2: multiple slow rates, with up to two additional (secondary and tertiary) slow trajectories on top of the primary driver changing over time (Fig. 2 multiple drivers).
- Experiment 3: the addition of noise to the primary trajectory (Fig. 3), with all other drivers held constant. The magnitude of noise may be either coupled or uncoupled from the trajectory of the primary driver.
- Experiment 4: the addition of noise to the primary driver, with up to two additional slow drivers (Fig. 4). The magnitude of noise may be either coupled or uncoupled from the trajectory of the primary driver.

To survey a wide range of future trajectories and generate a sufficient number of simulations that collapsed (Time-series breakpoint detection), each of the models were run for the following number of iterations (including both coupled and uncoupled settings):

- Lake Chilika fishery: 70,000
- Easter Island: 70,000
- TRIFFID: 70,000
- Lake Phosphorus: 120,000

In turn, to maximize computational efficiency both in STELLA and in R, the following logic was applied to the inbuilt Monte Carlo function

in STELLA to automatically generate the four different experiment types described above (the baseline primary driver always remains ‘on/active’):

- If  $\mu_1 > 0.4$  then secondary driver active else secondary driver remains at default value.
- If  $\mu_2 > 0.4$  then tertiary driver active else tertiary driver remains at default value.
- If  $\mu_3 > 0.4$  then noise active else noise level remains at zero.

Where  $\mu_1$ ,  $\mu_2$  and  $\mu_3$  represent ‘on switches’, with values randomly sampled from uniform distributions between 0 and 1 per simulation. The number of simulations per model experiment which showed ATDCs are detailed in Supplementary Table 3-1.

Whilst some insights could be obtained deterministically<sup>62</sup>, this is not possible for all models (for example, Lake Chilika) nor for all experiments (those involving additional noise). Thus, undertaking these model runs and analyses of the outputs (below) is the most consistent, feasible approach suitable across all models and experiments, allowing for comparisons across experiments, as well as investigation of synergistic impacts—fulfilling our primary aim of investigating the impact of the interaction of fast drivers, multiple drivers and system noise on the timing of tipping points in ecosystems.

To investigate experiment 1, each of the four models has one primary baseline driver which changes from its default value in every simulation:

- Lake Chilika fishery: fisher population growth rate (net difference between the birth rate per 1,000 population and the death rate per 1,000 population)
- Easter Island: tree clearance rate (trees per person per year)
- TRIFFID: local temperature (°C)
- Lake Phosphorus: phosphorus input rate (unitless)

Baseline outputs were generated with the primary driver active and the secondary and tertiary drivers remaining at its default value and the noise level remaining at zero (Supplementary Table 3-2). In turn, the Monte Carlo sensitivity analysis function in STELLA randomly samples a future change trajectory for the primary slow driver per simulation (as plotted on the horizontal axes of Figs. 2–4). The primary trajectory is sampled between the lower and upper limits of uniform distribution bounds, meaning that there is a uniform likelihood of selecting any given trajectory between the bounds (Supplementary Table 3-2). A future change trajectory of ‘0’ would cause no change from the default value; the maximum trajectory change limits for each of the models can be seen in Supplementary Table 3-2.

The built-in STELLA ‘TIME’ function generates future scenario trajectories that change linearly over time (with a constant gradient over the model horizon). Therefore, the value of the primary driver at any given timestep equals:

$$\text{Scenario value}_{i,t} = \text{TIME}_{i,t} \times \left( \frac{\text{Maximum trajectory value}_i}{\text{Total number of timesteps in model}} \right) \quad (3)$$

where  $i$  is the simulation number and  $t$  is the timestep (for example,  $t = 1, 2, 3, \dots$  total number of timesteps in model). Using the Easter Island model as an example: if a maximum tree clearance value of 7 has been sampled for the given simulation, then its value after 500 timesteps would be equal to  $500 \times (7/1,500) = 2.333$ . The plausible trajectory funnels for each of the primary drivers are plotted in Supplementary Fig. 3-1.

To simulate experiment 2, secondary and tertiary driver trajectories are also activated using the following logic:

- Secondary: primary driver active and secondary driver active and tertiary driver remains at default value and noise level remains at zero or

- Tertiary: primary driver active and secondary driver remains at default value and tertiary driver active and noise level remains at zero or
- All: primary driver active and secondary driver active and tertiary driver active and noise level remains at zero

For each model, this specifically involved the following variables (Supplementary Table 3-2):

- Lake Chilika fishery: (1) annual rainfall totals and mean near-surface air temperatures, as per IPCC (2013) climate change projections for the east coast of India; (2) price of fish per unit (Indian rupee per kg), leading to a more commercially oriented fishery, with an increasing number of fishers able to upgrade from traditional fishing boats to more intensive motorboats<sup>33</sup>.
- Easter Island: (1) agricultural carrying capacity of the system, which enables a higher human population to be supported per unit of land cleared for agriculture; (2) the mortality rate of trees as a proxy for a disease-spread event.
- TRIFFID: (1) temperature-independent disturbance rate of vegetation coverage, that is, causes of forest clearance which are not directly linked to temperature changes (for example, deforestation). Note: due to the small size of the model, TRIFFID does not have a tertiary driver.
- Lake Phosphorus: (1) rate of phosphorus recycling within the lake environment, (2) rate of phosphorus removal from the lake via sedimentation.

For the Lake Chilika and Easter Island models, these additional drivers are external forcings (similar to the primary driver). However, since the TRIFFID and Lake Phosphorus models are designed with only a single external forcing, additional drivers were also generated internally by altering parameters that operate on state variables. Whilst mathematically, internal and external forcings are fundamentally different things, both potentially impact the state of the system and, ecologically, changing internal model parameters can act as a proxy for an external process causing that change. For example, in the Lake Phosphorus model we have a system with a bifurcation in one dimension of slow external forcing ( $\alpha$ ) and we additionally vary internal parameters of the system (P recycling rate and P removal rate) as a proxy for, for example, anthropogenic disturbance impacting the species composition within the lake<sup>63</sup>.

Each of the additional driver trajectories are produced via the same approach as in equation (3): the Monte Carlo sensitivity analysis function in STELLA randomly samples a trajectory between the lower and upper bounds of a uniform distribution for each driver (Supplementary Table 3-2); in turn, the TIME function linearly increases the value of the driver from its default value to its sampled trajectory value by the final timestep of the model horizon.

To produce one secondary trajectory per simulation in the Lake Chilika model, the sampling of rainfall and temperature trajectories are connected along a linear gradient, ranging from no change to a combination of +30% rainfall change and +4.5 °C temperature change by 2081–2100 relative to 1986–2005 (as per representative concentration pathway 8.5 projections for the east coast of India<sup>64</sup>). In STELLA, this is operationalized by the model variable ‘climate change trend’, with Monte Carlo sensitivity analysis in STELLA randomly sampling a value between 0 and 1 per simulation. As an illustration, if a value of 0.6 was to be sampled, then the change in rainfall by 2081–2100 (relative to 1986–2005) would equal  $0.6 \times 30(\%) = 18\%$ , whilst the change in temperature would equal  $0.6 \times 4.5(^{\circ}\text{C}) = 2.7^{\circ}\text{C}$ .

To investigate experiments 3 and 4, the value of each primary slow driver is perturbed per timestep by randomly generated noise. We simulate a standard Wiener process to generate noise, equal to  $\sqrt{dt} \times N(0,1)$ , where ‘dt’ equals change in time and ‘N(0,1)’ is a normal

distribution with a mean of 0 and standard deviation of one. In turn, the product of the Wiener process is multiplied by the scaling factor  $\sigma$ , providing an overall level of noise to be added to the value of the primary driver on any given timestep. As per the future trajectories, the magnitude of  $\sigma$  is randomly sampled once per simulation from uniform distributions, with lower and upper limits shown in Supplementary Table 3-2.

Therefore, building on equation (3) above, the value of a primary driver at any point in time in experiments 3 and 4 equals:

$$\text{Scenario value}_{i,t} = \text{TIME}_{i,t} \times \left( \frac{\text{Maximum trajectory value}_i}{\text{Total number of timesteps in model}} \right) + \left( \sigma_i \times \sqrt{dt} \times N(0,1)_t \right) \quad (4)$$

Equation (4) as detailed above only refers to the ‘uncoupled’ noise simulations. Therefore, to explore the effects of ‘coupled’ noise, whereby the magnitude of noise increases with the growth in the primary driver, 20,000 simulations were run per model spread evenly between experiments 3 and 4, with the magnitude of noise coupled to the magnitude of the primary driver trajectory. Given the differences in the shape of the noise spectrums, we do not directly compare outcomes from the uncoupled and coupled noise simulations in this study. Instead, the purpose of modelling coupled noise is to ascertain whether worsening magnitudes of extreme events over time are associated with earlier ATDCs. In the coupled simulations, equation (4) is modified to:

$$\text{Scenario value}_{i,t} = \text{TIME}_{i,t} \times \left( \frac{\text{Maximum trajectory value}_i}{\text{Total number of timesteps in model}} \right) + \left( \sigma_i \times \sqrt{dt} \times N(0,1)_t \times \text{Change in scenario value from default}_{i,t} \right) \quad (5)$$

For experiment 3 (single slow driver plus noise), the runs were generated in STELLA<sup>39</sup> with the following logic: primary driver active and secondary driver remains at default value and tertiary driver remains at default value and noise active. For experiment 4 (noise plus multiple slow drivers), the logic used included:

- Primary driver active and secondary driver active and tertiary driver remains at default value and noise active.
- Primary driver active and secondary driver remains at default value and tertiary driver active and noise active.
- Primary driver active and secondary driver active and tertiary driver active and noise active.

### Time-series breakpoint detection

The identification of the timing of the ATDCs in the model runs was a two-step process.

First, to ensure that we were only analysing model runs that had transitioned (collapsed) to quantitatively and qualitatively functionally different states (for example, fishery collapse, civilization collapse, forest dieback or lake eutrophication), we assessed whether model outcomes had crossed a predefined threshold at any point over the model horizon. For the three models which observe collapses in the outcome variable (Lake Chilika fishery, Easter Island and TRIFFID), model runs were considered to have reached a collapsed state if the outcome variable reached a value beneath 20% of its initial value at any point during the simulation. This demarcation is therefore representative of type-1 boundaries defined by ref. 40, with the numerical value of the boundary in line with the concept that fish stocks may be considered collapsed once their biomass falls beneath 20% of the biomass needed to maintain maximum sustainable yield<sup>65,66</sup>. In the case of the Lake Chilika fishery model, which has inbuilt social-ecological feedbacks that may trigger the recovery and later recollapse of the fishery<sup>21,33</sup>, we subset the time series to the period before the first timestep beneath 20% of the initial fish population. As we are only interested in the initial collapse, not

subsetting this time period would risk capturing subsequent collapses and recoveries in the analysis.

With lake eutrophication caused by an increase in phosphorus concentrations, a linear threshold beyond which we could be confident that the model had entered a qualitatively different state could not be identified. Therefore, as per the approach taken by ref. 67 for identifying abrupt events in global climate models, we adopted a ref. 40 type-2 boundary to include only simulations which reached lake phosphorus concentrations greater than four times the standard deviation (s.d.) of the pre-ATDC time series. Therefore, runs of the Lake Phosphorus model which did not exceed this  $4 \times$  s.d. threshold were not considered to reach phosphorus concentrations sufficiently outside of the pretransition envelope of variability and were therefore excluded from our analysis.

The second stage of time-series breakpoint detection used the optimal breakpoint function of the R package *strucchange* v.1.5-2 (ref. 68) to identify ATDC dates in the time series that had successfully met the above qualifications (that is, reached an alternative state). As described in ref. 21, the optimal breakpoint function finds the most substantial deviation from stability in classical regression models (Supplementary Fig. 3-2), whereby regressions coefficients shift from one regime to another. Therefore, the breakpoint date is taken as the most substantial deviation of the outcome variable en route to its qualitatively and quantitatively alternative state.

### Boxplots and output graphs

For each of the experiments (Generation of future scenarios), boxplots were generated to visualize the distribution of breakpoint dates for each of the slow driver and noise level combinations (Figs. 2–4). To standardize the comparisons between experiments, the normalized magnitude ( $0 \rightarrow 1$ ) of the primary trajectories (Supplementary Table 3-2) for each model was plotted on the horizontal axes. In turn, to visualize how the breakpoint dates change with the addition of secondary or noisy stresses over the range of the primary trajectories, model outcomes that tipped (Time-series breakpoint detection) were subset in the statistical software R between normalized primary trajectory values of 0.25–0.35, 0.45–0.55 and 0.65–0.75. From here, boxplots for each of the driver combinations (for example, ‘primary only’ and ‘primary and secondary’) and primary driver subsets (for example, 0.25–0.35 and 0.45–0.55) were graphed in R using the package *ggplot* (v.3.3.5; ref. 69).

### Inclusion and ethics statement

This research is global in scope, using models that have been appropriately cited throughout. Roles and responsibilities were agreed amongst collaborators ahead of the research.

### Reporting summary

Further information on research design is available in the Nature Portfolio Reporting Summary linked to this article.

### Data availability

The datasets generated during and/or analysed during the current study are available from the corresponding author on reasonable request, with the models used to create these data available in a DOI-minting repository: <https://doi.org/10.5281/zenodo.7946433>.

### Code availability

The code used to analyse the modelled data are deposited in a DOI-minting repository: <https://doi.org/10.5281/zenodo.7946433>.

### References

- Beddington, J. *Food, Energy, Water and the Climate: A Perfect Storm of Global Events* (Government Office for Science, 2009).
- Bradshaw, C. J. A. et al. Underestimating the challenges of avoiding a ghastly future. *Front. Conserv. Sci.* **1**, 615419 (2021).
- Retsa, A., Schelske, O., Wilke, B., Rutherford, G. & de Jong, R. *Biodiversity and Ecosystem Services: A Business Case for Re/insurance* (Swiss Re Institute, 2020); <https://www.swissre.com/institute/research/topics-and-risk-dialogues/climate-and-natural-catastrophe-risk/expertise-publication-biodiversity-and-ecosystems-services>
- Reichstein, M., Riede, F. & Frank, D. More floods, fires and cyclones—plan for domino effects on sustainability goals. *Nature* **592**, 347–349 (2021).
- Scheffer, M. et al. Anticipating critical transitions. *Science* **338**, 344–348 (2012).
- Kareiva, P. & Carranza, V. Existential risk due to ecosystem collapse: nature strikes back. *Futures* **102**, 39–50 (2018).
- Kemp, L. et al. Climate endgame: exploring catastrophic climate change scenarios. *Proc. Natl Acad. Sci. USA* **119**, e2108146119 (2022).
- Steffen, W. et al. Planetary boundaries: guiding human development on a changing planet. *Science* <https://doi.org/10.1126/science.1259855> (2015).
- Ripple, W. J., Wolf, C., Newsome, T. M., Barnard, P. & Moomaw, W. R. World scientists’ warning of a climate emergency. *Bioscience* **70**, 8–12 (2020).
- Global Biodiversity Outlook 5* (Convention on Biological Diversity, 2020); [www.cbd.int/GBO5](http://www.cbd.int/GBO5)
- IPCC. *Climate Change 2021: The Physical Science Basis* (eds Masson-Delmotte, V. et al.) (Cambridge Univ. Press, 2021).
- Büntgen, U. et al. Recent European drought extremes beyond Common Era background variability. *Nat. Geosci.* **14**, 190–196 (2021).
- Abram, N. J. et al. Connections of climate change and variability to large and extreme forest fires in southeast Australia. *Commun. Earth Environ.* **2**, 8 (2021).
- Toreti, A., Cronie, O. & Zampieri, M. Concurrent climate extremes in the key wheat producing regions of the world. *Sci. Rep.* **9**, 5493 (2019).
- Vogel, M. M., Hauser, M. & Seneviratne, S. I. Projected changes in hot, dry and wet extreme events’ clusters in CMIP6 multi-model ensemble. *Environ. Res. Lett.* **15**, 094021 (2020).
- Gaupp, F., Hall, J., Mitchell, D. & Dadson, S. Increasing risks of multiple breadbasket failure under 1.5 and 2°C global warming. *Agric. Syst.* **175**, 34–45 (2019).
- McKay, D. I. A. et al. Exceeding 1.5°C global warming could trigger multiple climate tipping points. *Science* **377**, eabn7950 (2022).
- Siteur, K., Eppinga, M. B., Doelman, A., Siero, E. & Rietkerk, M. Ecosystems off track: rate-induced critical transitions in ecological models. *Oikos* **125**, 1689–1699 (2016).
- Ashwin, P., Wieczorek, S., Vitolo, R. & Cox, P. Tipping points in open systems: bifurcation, noise-induced and rate-dependent examples in the climate system. *Philos. Trans. R. Soc. A* **370**, 1166–1184 (2012).
- O’Keeffe, P. E. & Wieczorek, S. Tipping phenomena and points of no return in ecosystems: beyond classical bifurcations. *SIAM J. Appl. Dyn. Syst.* **19**, 2371–2402 (2019).
- Cooper, G. S., Willcock, S. & Dearing, J. A. Regime shifts occur disproportionately faster in larger ecosystems. *Nat. Commun.* **11**, 1175 (2020).
- Arani, B. M. S., Carpenter, S. R., Lahti, L., Van Nes, E. H. & Scheffer, M. Exit time as a measure of ecological resilience. *Science* **372**, eaay4895 (2021).
- Thompson, J. M. T. & Sieber, J. Predicting climate tipping as a noisy bifurcation: a review. *Int. J. Bifurc. Chaos* **21**, 399–423 (2011).
- Wilson, W. G. Resolving discrepancies between deterministic population models and individual-based simulations. *Am. Nat.* **151**, 116–134 (1998).

25. Thompson, R. M., Beardall, J., Beringer, J., Grace, M. & Sardina, P. Means and extremes: building variability into community-level climate change experiments. *Ecol. Lett.* **16**, 799–806 (2013).
26. Kreyling, J., Jentsch, A. & Beier, C. Beyond realism in climate change experiments: gradient approaches identify thresholds and tipping points. *Ecol. Lett.* <https://doi.org/10.1111/ele.12193> (2014).
27. Ritchie, P. D. L., Clarke, J. J., Cox, P. M. & Huntingford, C. Overshooting tipping point thresholds in a changing climate. *Nature* **592**, 517–523 (2021).
28. Wang, R. et al. Flickering gives early warning signals of a critical transition to a eutrophic lake state. *Nature* **492**, 419–422 (2012).
29. Groffman, P. M. et al. Ecological thresholds: the key to successful environmental management or an important concept with no practical application? *Ecosystems* **9**, 1–13 (2006).
30. Renaud, F. G., Birkmann, J., Damm, M. & Gallopin, G. C. Understanding multiple thresholds of coupled social–ecological systems exposed to natural hazards as external shocks. *Nat. Hazards* **55**, 749–763 (2010).
31. Kelly, R. A. et al. Selecting among five common modelling approaches for integrated environmental assessment and management. *Environ. Model. Softw.* **47**, 159–181 (2013).
32. Filatova, T., Polhill, J. G. & van Ewijk, S. Regime shifts in coupled socio-environmental systems: review of modelling challenges and approaches. *Environ. Model. Softw.* **75**, 333–347 (2016).
33. Cooper, G. S. & Dearing, J. A. Modelling future safe and just operating spaces in regional social-ecological systems. *Sci. Total Environ.* **651**, 2105–2117 (2019).
34. Tenza, A., Pérez, I., Martínez-Fernández, J. & Giménez, A. Understanding the decline and resilience loss of a long-lived social-ecological system: insights from system dynamics. *Ecol. Soc.* **22**, 15 (2017).
35. Martin, R. & Schlüter, M. Combining system dynamics and agent-based modeling to analyze social-ecological interactions—an example from modeling restoration of a shallow lake. *Front. Environ. Sci.* **3**, 66 (2015).
36. Brandt, G. & Merico, A. The slow demise of Easter Island: insights from a modeling investigation. *Front. Ecol. Evol.* **3**, 13 (2015).
37. Carpenter, S. R., Ludwig, D. & Brock, W. A. Management of eutrophication for lakes subject to potentially irreversible change. *Ecol. Appl.* **9**, 751–771 (1999).
38. Cox, P. M. et al. Amazonian forest dieback under climate-carbon cycle projections for the 21st century. *Theor. Appl. Climatol.* **78**, 137–156 (2004).
39. *STELLA Architect: Systems Thinking for Education and Research* (ISEE Systems, 2018); <https://www.iseesystems.com/about.aspx>
40. Dearing, J. A. et al. Safe and just operating spaces for regional social-ecological systems. *Glob. Environ. Change* **28**, 227–238 (2014).
41. Krönke, J. et al. Dynamics of tipping cascades on complex networks. *Phys. Rev. E* **101**, 042311 (2020).
42. Kinzig, A. P. et al. Resilience and regime shifts: assessing cascading effects. *Ecol. Soc.* **11**, 20 (2006).
43. Klose, A. K., Karle, V., Winkelmann, R. & Donges, J. F. Emergence of cascading dynamics in interacting tipping elements of ecology and climate. *R. Soc. Open Sci.* **7**, 200599 (2020).
44. Wang, R., Dearing, J. A. & Langdon, P. G. Critical transitions in ecosystem state are driven by coupled feedback mechanisms: a case study from Erhai lake, China. *Water* **13**, 85 (2022).
45. Rietkerk, M. et al. Evasion of tipping in complex systems through spatial pattern formation. *Science* **374**, 6564 (2021).
46. Bastiaansen, R., Dijkstra, H. A. & Von Der Heydt, A. S. Fragmented tipping in a spatially heterogeneous world. *Environ. Res. Lett.* **17**, 045006 (2022).
47. Dearing, J. A. et al. Navigating the perfect storm: research strategies for social ecological systems in a rapidly evolving world. *Environ. Manag.* **49**, 767–775 (2011).
48. Verburg, P. H. et al. Methods and approaches to modelling the Anthropocene. *Glob. Environ. Change* **39**, 328–340 (2016).
49. Beven, K. A manifesto for the equifinality thesis. *J. Hydrol.* **320**, 18–36 (2006).
50. Reisinger, D. & Füllsack, M. Comparing equation-based and agent-based data generation methods for early warning signal analysis. *Systems* **8**, 54 (2020).
51. Scheffer, M. et al. Early-warning signals for critical transitions. *Nature* **461**, 53–59 (2009).
52. Bury, T. M. et al. Deep learning for early warning signals of tipping points. *Proc. Natl Acad. Sci. USA* **118**, e2106140118 (2021).
53. Doncaster, C. P. et al. Early warning of critical transitions in biodiversity from compositional disorder. *Ecology* **97**, 3079–3090 (2016).
54. Wang, R. et al. Network parameters quantify loss of assemblage structure in human-impacted lake ecosystems. *Glob. Change Biol.* **25**, 3871–3882 (2019).
55. Mayfield, R. J. et al. Metrics of structural change as indicators of chironomid community stability in high latitude lakes. *Quat. Sci. Rev.* **249**, 106594 (2020).
56. Cai, Y., Lenton, T. M. & Lontzek, T. S. Risk of multiple interacting tipping points should encourage rapid CO<sub>2</sub> emission reduction. *Nat. Clim. Change* **6**, 520–525 (2016).
57. Dietz, S., Rising, J., Stoerk, T. & Wagner, G. Economic impacts of tipping points in the climate system. *Proc. Natl Acad. Sci. USA* **118**, e21030811 (2021).
58. Fabbri, S., Hauschild, M. Z., Lenton, T. M. & Owsianiak, M. Multiple climate tipping points metrics for improved sustainability assessment of products and services. *Environ. Sci. Technol.* **55**, 2800–2810 (2021).
59. Steffen, W., Broadgate, W., Deutsch, L., Gaffney, O. & Ludwig, C. The trajectory of the Anthropocene: the Great Acceleration. *Anthr. Rev.* **2**, 81–98 (2015).
60. R Core Team. *R: A Language and Environment for Statistical Computing* (R Foundation for Statistical Computing, 2020).
61. Carpenter, S. R. Eutrophication of aquatic ecosystems: bistability and soil phosphorus. *Proc. Natl Acad. Sci. USA* **102**, 10002–10005 (2005).
62. Rheinboldt, W. C. *Methods for Solving Systems of Nonlinear Equations* (Society for Industrial and Applied Mathematics, 1998).
63. Huang, S., Zhang, K., Lin, Q., Liu, J. B. & Shen, J. Abrupt ecological shifts of lakes during the Anthropocene. *Earth Sci. Rev.* **227**, 103981 (2022).
64. IPCC. *Climate Change 2013: The Physical Science Basis* (eds Stocker, T. F. et al.) (Cambridge Univ. Press, 2013).
65. Worm, B. et al. Rebuilding global fisheries. *Science* **325**, 578–585 (2009).
66. Pinsky, M. L., Jensen, O. P., Ricard, D. & Palumbi, S. R. Unexpected patterns of fisheries collapse in the world's oceans. *Proc. Natl Acad. Sci. USA* **108**, 8317–8322 (2011).
67. Drijfhout, S. et al. Catalogue of abrupt shifts in Intergovernmental Panel on Climate Change climate models. *Proc. Natl Acad. Sci. USA* **112**, E5777–E5786 (2015).
68. Zeileis, A., Leisch, F., Hornik, K. & Kleiber, C. Package “strucchange”. R package version 1.5-2 <https://cran.r-project.org/web/packages/strucchange/strucchange.pdf> (2015).
69. Wickham, H. *ggplot2: Elegant Graphics for Data Analysis* (Springer, 2016).

## Acknowledgements

S.W. received funding from NE/WO05050/1, NE/T00391X/1, ES/T007877/1, ES/R009279/1, AH/WO03813/1 and BB/X010961/1. G.S.C.

received funding by the UKRI-GCRF Action Against Stunting Hub (project ref. MR/S01313X/1).

### Author contributions

S.W., G.S.C. and J.A.D. conceived and wrote the manuscript. G.S.C. ran and analysed the models. J.A. provided statistically support and conceptualized the figures. All authors edited and approved the final manuscript.

### Competing interests

The authors declare no competing interests.

### Additional information

**Supplementary information** The online version contains supplementary material available at <https://doi.org/10.1038/s41893-023-01157-x>.

**Correspondence and requests for materials** should be addressed to Simon Willcock.

**Peer review information** *Nature Sustainability* thanks Max Rietkerk and the other, anonymous, reviewer(s) for their contribution to the peer review of this work.

**Reprints and permissions information** is available at [www.nature.com/reprints](http://www.nature.com/reprints).

**Publisher's note** Springer Nature remains neutral with regard to jurisdictional claims in published maps and institutional affiliations.

**Open Access** This article is licensed under a Creative Commons Attribution 4.0 International License, which permits use, sharing, adaptation, distribution and reproduction in any medium or format, as long as you give appropriate credit to the original author(s) and the source, provide a link to the Creative Commons license, and indicate if changes were made. The images or other third party material in this article are included in the article's Creative Commons license, unless indicated otherwise in a credit line to the material. If material is not included in the article's Creative Commons license and your intended use is not permitted by statutory regulation or exceeds the permitted use, you will need to obtain permission directly from the copyright holder. To view a copy of this license, visit <http://creativecommons.org/licenses/by/4.0/>.

© The Author(s) 2023

## Reporting Summary

Nature Portfolio wishes to improve the reproducibility of the work that we publish. This form provides structure for consistency and transparency in reporting. For further information on Nature Portfolio policies, see our [Editorial Policies](#) and the [Editorial Policy Checklist](#).

### Statistics

For all statistical analyses, confirm that the following items are present in the figure legend, table legend, main text, or Methods section.

- | n/a                                 | Confirmed  |
|-------------------------------------|--|
| <input type="checkbox"/>            | <input checked="" type="checkbox"/> The exact sample size ( $n$ ) for each experimental group/condition, given as a discrete number and unit of measurement  |
| <input type="checkbox"/>            | <input checked="" type="checkbox"/> A statement on whether measurements were taken from distinct samples or whether the same sample was measured repeatedly  |
| <input checked="" type="checkbox"/> | <input type="checkbox"/> The statistical test(s) used AND whether they are one- or two-sided<br><i>Only common tests should be described solely by name; describe more complex techniques in the Methods section.</i>  |
| <input type="checkbox"/>            | <input checked="" type="checkbox"/> A description of all covariates tested   |
| <input checked="" type="checkbox"/> | <input type="checkbox"/> A description of any assumptions or corrections, such as tests of normality and adjustment for multiple comparisons   |
| <input type="checkbox"/>            | <input checked="" type="checkbox"/> A full description of the statistical parameters including central tendency (e.g. means) or other basic estimates (e.g. regression coefficient) AND variation (e.g. standard deviation) or associated estimates of uncertainty (e.g. confidence intervals) |
| <input checked="" type="checkbox"/> | <input type="checkbox"/> For null hypothesis testing, the test statistic (e.g. $F$ , $t$ , $r$ ) with confidence intervals, effect sizes, degrees of freedom and $P$ value noted<br><i>Give <math>P</math> values as exact values whenever suitable.</i>                                       |
| <input checked="" type="checkbox"/> | <input type="checkbox"/> For Bayesian analysis, information on the choice of priors and Markov chain Monte Carlo settings  |
| <input checked="" type="checkbox"/> | <input type="checkbox"/> For hierarchical and complex designs, identification of the appropriate level for tests and full reporting of outcomes  |
| <input checked="" type="checkbox"/> | <input type="checkbox"/> Estimates of effect sizes (e.g. Cohen's $d$ , Pearson's $r$ ), indicating how they were calculated  |

*Our web collection on [statistics for biologists](#) contains articles on many of the points above.*

### Software and code

Policy information about [availability of computer code](#)

- |                 |   |
|-----------------|---|
| Data collection | We run four previously published models. Each model was replicated and simulated within the system dynamics software STELLA Architect v.1.6.151. The models are available here: <a href="https://doi.org/10.5281/zenodo.7946433">https://doi.org/10.5281/zenodo.7946433</a>   |
| Data analysis   | Outputs were exported into CSV files as time series and analysed in the statistical software R v.4.1.0. The optimal breakpoint function of the R package 'strucchange' v.1.5-2 was used. Boxplots were graphed in R using the package 'ggplot' (v.3.3.5). The code supporting this is available here: <a href="https://doi.org/10.5281/zenodo.7946433">https://doi.org/10.5281/zenodo.7946433</a> |

For manuscripts utilizing custom algorithms or software that are central to the research but not yet described in published literature, software must be made available to editors and reviewers. We strongly encourage code deposition in a community repository (e.g. GitHub). See the Nature Portfolio [guidelines for submitting code & software](#) for further information.

### Data

Policy information about [availability of data](#)

All manuscripts must include a [data availability statement](#). This statement should provide the following information, where applicable:

- Accession codes, unique identifiers, or web links for publicly available datasets
- A description of any restrictions on data availability
- For clinical datasets or third party data, please ensure that the statement adheres to our [policy](#)

The datasets generated during and/or analysed during the current study are available from <https://doi.org/10.5281/zenodo.7946433>

## Human research participants

Policy information about [studies involving human research participants and Sex and Gender in Research](#).

Reporting on sex and gender	n/a
Population characteristics	n/a
Recruitment	n/a
Ethics oversight	n/a

Note that full information on the approval of the study protocol must also be provided in the manuscript.

## Field-specific reporting

Please select the one below that is the best fit for your research. If you are not sure, read the appropriate sections before making your selection.

Life sciences     Behavioural & social sciences     Ecological, evolutionary & environmental sciences

For a reference copy of the document with all sections, see [nature.com/documents/nr-reporting-summary-flat.pdf](https://nature.com/documents/nr-reporting-summary-flat.pdf)

## Ecological, evolutionary & environmental sciences study design

All studies must disclose on these points even when the disclosure is negative.

Study description	We aim to generalise the dynamics of increasing the numbers of drivers, their rates and variability (as proxies for stronger interactions between systems and noise) on the speed at which tipping points are reached in four model social-ecological system dynamics models: Chilika fishery, Lake phosphorus, Easter Island, and a modified version of The Hadley Centre Dynamic Global Vegetation Model (TRIFFID) of forest dieback.
Research sample	The Chilika fishery model is a social-ecological model designed to simulate the future fish population and catch trajectories of the Chilika lagoon, Odisha, India. The Lake phosphorus model is a simplified version of the original 'lake response to P input and recycling' model, as modified by Wang et al. (48). The Easter Island model aims to explore alternative hypotheses behind the social-ecological collapse of the Easter Island civilisation. The TRIFFID model is a modified version of The Hadley Centre Dynamic Global Vegetation Model, originally developed by Cox et al. (50) to explore the effects of atmospheric CO <sub>2</sub> concentrations on the rate of Amazon dieback.
Sampling strategy	We performed four in silico experiments: <ul style="list-style-type: none"> <li>– Experiment #1: only the primary slow driver in each model changes over time, and all other drivers remain constant;</li> <li>– Experiment #2: multiple slow rates, with up to two additional (i.e. 'secondary' and 'tertiary') slow trajectories on top of the primary driver changing over time;</li> <li>– Experiment #3: the addition of noise to the primary trajectory, with all other drivers held constant. The magnitude of noise may be either coupled or uncoupled from the trajectory of the primary driver;</li> <li>– Experiment #4: the addition of noise to the primary driver, with up to two additional slow drivers. The magnitude of noise may be either coupled or uncoupled from the trajectory of the primary driver .</li> </ul> Each of the models were ran for the following number of iterations (including both 'coupled' and 'uncoupled' settings): <ul style="list-style-type: none"> <li>– Chilika fishery: 70,000</li> <li>– Easter Island: 70,000</li> <li>– Lake Phosphorus: 120,000</li> <li>– TRIFFID: 70,000</li> </ul>
Data collection	All data are modelled from the above experiments.
Timing and spatial scale	All data are modelled from the above experiments. The time and spatial scale of the models vary
Data exclusions	This research focusses on tipping points, so only model runs that went through Type-1 or Type-2 boundaries defined by Dearing et al. (14) were included in the analysis
Reproducibility	Being modelled, the data are fully reproducible.
Randomization	Being modelled, we have full control of covariates and so randomisation is not necessary
Blinding	Blinding is not relevant to this study. Our data are identified using the optimal breakpoint function of the R package 'strucchange' v.1.5-2 and so observer bias is not possible

Did the study involve field work?  Yes  No

## Reporting for specific materials, systems and methods

We require information from authors about some types of materials, experimental systems and methods used in many studies. Here, indicate whether each material, system or method listed is relevant to your study. If you are not sure if a list item applies to your research, read the appropriate section before selecting a response.

### Materials & experimental systems

- | n/a                                 | Included in the study                                  |
|-------------------------------------|--|
| <input checked="" type="checkbox"/> | <input type="checkbox"/> Antibodies                    |
| <input checked="" type="checkbox"/> | <input type="checkbox"/> Eukaryotic cell lines         |
| <input checked="" type="checkbox"/> | <input type="checkbox"/> Palaeontology and archaeology |
| <input checked="" type="checkbox"/> | <input type="checkbox"/> Animals and other organisms   |
| <input checked="" type="checkbox"/> | <input type="checkbox"/> Clinical data                 |
| <input checked="" type="checkbox"/> | <input type="checkbox"/> Dual use research of concern  |

### Methods

- | n/a                                 | Included in the study                           |
|-------------------------------------|---|
| <input checked="" type="checkbox"/> | <input type="checkbox"/> ChIP-seq               |
| <input checked="" type="checkbox"/> | <input type="checkbox"/> Flow cytometry         |
| <input checked="" type="checkbox"/> | <input type="checkbox"/> MRI-based neuroimaging |